C.P. No. 1253

C.P. No. 1253

PROCUREMENT EXECUTIVE, MINISTRY OF DEFENCE

AERONAUTICAL RESEARCH COUNCIL

CURRENT PAPERS

A Technique for Measuring Oscillatory Aerodynamic Control Surface Hinge Moments from Forced Response Characteristics

by

D. R. Gaukroger, D A. Drane and R. Gray

Structures Dept., R.A.E., Farnborough

LONDON: HER MAJESTY'S STATIONERY OFFICE

1973

PRICE 60*p* NET

UDC 533.6.013.155 : 533.694.5 : 533.6.013.42 : 533.6.011.35

CP No.1253 *
October 1971

A TECHNIQUE FOR MEASURING OSCILLATORY AERODYNAMIC CONTROL SURFACE HINGE MOMENTS FROM FORCED RESPONSE CHARACTERISTICS

by

D. R. Gaukroger
D. A. Drane
R. Gray

SUMMARY

A technique for measuring the hinge moment aerodynamic derivatives for an oscillating control surface is described. The technique is identical to that used in the measurement of subcritical response of flutter models, except that the model under test is nominally rigid, and the only designed motion is rotation of the control surface. Test results are given for a full-span control surface on a slightly swept wing. The Mach number range was from M = 0.6 to M = 1.2, and the Reynolds number range from 0.7 to 2.7 million, based on wing mean chord.

* Replaces RAE Technical Report 71211 - ARC 33869

CONTENTS

1 INTRODUCTION

In 1969, an ARC Working Party on unsteady aerodynamics reviewed the work in progress pertaining to flutter, and made a number of recommendations for future work[1]. The Working Party endorsed an RAE proposal for the development of a simple rig to measure the oscillatory hinge moments h_β and $h_{\dot\beta}$, and the purpose of this Report is to describe the rig that has been developed and to record results that have been obtained.

The design aims for the rig were:-

(i) simplicity of construction, instrumentation and operation,

(ii) capability of obtaining test data over a wide range of Mach number, Reynolds number and frequency parameter,

(iii) as high an order of accuracy as possible in the measured derivatives consistent with a simple rig design.

The implication in (iii), above, that some reduction in accuracy would be acceptable as the price for simplicity, was quite deliberate, and was based on the belief that when there is a need, within a given timescale and cost, to obtain hinge moment data for a particular planform, it is more useful to cover a wide range of parameter variations with moderate accuracy in the measured data, than a narrow range with high accuracy. Not only would this be advantageous in relation to projects, but it would also enable exploration of hinge moment variations to be made much more fully and rapidly in research investigations than is normally possible.

The rig that has been developed satisfies the design aims, and it is believed that the accuracy of the test results is, in general, as high as that obtained from more complex measurement techniques. Nevertheless, there is room for improvement in a number of respects, which are discussed in the Report.

Measured values of hinge moment derivatives are presented for a slightly swept wing with a full-span control surface over the range of Mach number from 0.6 to 1.2.

2 PRINCIPLE OF RIG DESIGN

The wide and successful use that has been made in recent years of the forced response and vector plot technique for measuring the natural frequency and damping of the modes of aeroelastic models suggests that the same technique could be used to obtain values of oscillatory aerodynamic derivatives. In particular, the technique would appear to be readily applicable

to the measurement of control surface hinge moment derivatives h_β and $h_{\dot\beta}$ (the hinge moment stiffness and damping derivatives due to control surface rotation). Equipment that will provide a sinusoidal force input to a structure and measure the variation with frequency of the structural response vector is readily available. The problem, then, is almost wholly one of rig design.

For a given size of model and flow velocity, the test frequency is determined by the value of the non-dimensional frequency parameter for which the aerodynamic derivatives are required. For a typical size of model in the RAE 3ft × 3ft tunnel at Bedford, operating at high subsonic Mach number, the control surface must oscillate at approximately 250 Hz to achieve values of frequency parameter of unity (based on wing chord). The simplest scheme is that shown in Fig.1, in which a control surface is attached to one end of a torsion bar whilst the other end of the bar is attached to an 'earth' point. Assuming that the control is effectively rigid at the frequencies under consideration, the equation of motion may be written:-

$$I_\beta + (d_s + d_a)\dot\beta + (k_s + k_a)\beta = M \sin \Omega t \qquad (1)$$

where M is the amplitude of an external moment applied to the system

Ω is the frequency of excitation

β is the angle of rotation of the control,

I is the moment of inertia of the system,

d_s and k_s are the structural damping and stiffness coefficients respectively,

d_a and k_a are the coefficients of the components of aerodynamic hinge moment, in quadrature and in phase, respectively, with the control rotation.

The undamped natural frequency (ω_r) and fraction of critical damping (μ_r) are given by:-

$$\omega_r^2 = \frac{k_a + k_s}{I} \qquad (2)$$

$$\mu_r = \frac{d_a + d_s}{2I\omega} \quad . \qquad (3)$$

When $d_a = k_a = 0$ (i.e. *in vacuo*):-

(4)

$$\omega_0^2 = \frac{k_s}{I} \tag{4}$$

$$\mu_0 = \frac{d_s}{2I\omega_0} \quad . \tag{5}$$

Hence:-

$$k_a = I(\omega_r^2 - \omega_0^2) \tag{6}$$

$$d_a = 2I(\omega_r\mu_r - \omega_0\mu_0) \quad . \tag{7}$$

For oscillatory motion the aerodynamic hinge moment H is given by:-

$$H = \rho V^2 sc^2(i\nu h_{\dot{\beta}} + h_\beta)\beta \tag{8}$$

where ρ, V are air density and velocity respectively,
s, c are wing span and mean chord respectively,
ν is non-dimensional frequency parameter $\left(= \frac{\omega c}{V}\right)$.

Since also, by definition, $H = -(d_a\dot{\beta} + k_a\beta)$, it follows that:-

$$d_a = -\rho V sc^3 h_{\dot{\beta}} \tag{9}$$

$$k_a = -\rho V^2 sc^2 h_\beta \tag{10}$$

hence,

$$(-h_{\dot{\beta}}) = \frac{2I(\omega_r\mu_r - \omega_0\mu_0)}{\rho V sc^3} \tag{11}$$

and

$$(-h_\beta) = \frac{I(\omega_r^2 - \omega_0^2)}{\rho V^2 sc^2} \quad . \tag{12}$$

From equations (11) and (12) it can be seen that, for maximum change of frequency and damping in any given aerodynamic condition, I and μ_0 should be as small as possible; ω_r (and hence ω_0) is, of course, determined by the value of frequency parameter for which values of the derivative are required.

3 PRACTICAL ASPECTS OF RIG DESIGN

3.1 Model and rig rigidity

One of the most difficult problems to be overcome in designing the test rig is that of ensuring that unwanted motions do not occur. With an operating frequency of 250 Hz, it is difficult to design the wing and control structure so that the only motion is rotation of the control. A design aim is to ensure that natural frequencies are well above the operating frequency, or, if this proves impossible, that the natural frequencies are well away from the operating frequency. Equally important is that oscillatory force inputs to any of the components should be minimal (except, of course, the forces required to drive the rig).

It is clear that the control surface must be supported at both the inner and outer extremities to avoid significant bending, since it will not generally be possible to design a control to behave as an effectively rigid cantilever. It is also necessary to make the control as light and as stiff as possible both to satisfy the inertia requirements of section 2 and to ensure that there is a minimum of distortion at the operating frequency. In particular, the fundamental torsional frequency of the control must be high because the excitation will tend to excite the control in twist.

The prevention of wing motion is, perhaps, the most difficult design problem. The wing will experience excitation from both mechanical and aerodynamic sources; the former will arise mainly from the support of the outer end of the control and, to a lesser extent, from the control leading edge gap seal, whilst the latter will arise from the oscillatory aerodynamic couplings. Naturally, the wing must be designed so that there are no resonance frequencies near the operating frequency, but even so it is probable that the response of the wing to the force input at the control hinge will result in a level of wing motion that will cast doubt on the validity of the measured control surface derivatives. A possible way of avoiding this difficulty is to prevent motion of the wing by means of taut wires between the wing and the tunnel walls. At first sight, this solution is one that is unlikely to meet with much approval on general aerodynamic grounds, particularly in high subsonic and transonic regimes where rapid changes in aerodynamic derivatives may be expected and where, therefore, flow disturbances should be kept to a minimum. Nevertheless it seems to the authors that if it can be shown that tethering the wing at a suitable point, or points, has only a small effect aerodynamically on

the oscillatory control hinge moments, it is a solution that should be adopted. The alternative, of designing the wing to be effectively rigid at operating frequencies that will inevitably be of the same order as the wing resonance frequencies (even if frequency coincidence can be avoided), is also exceedingly difficult. There is also the possibility of measuring whatever wing motion may occur and in some way making a correction for this motion in evaluating the hinge moment derivatives. In fact, such a procedure must be discounted as unacceptable, not only because of the complications that would be involved in mode measurement, but because the subsequent analyses would depend on a knowledge of all the aerodynamic derivatives associated with combined wing and control motion.

Thus, tethering the wing to prevent wing motion should be looked at as a means of obtaining the required aerodynamic data to greater accuracy than can otherwise be achieved. The validity of this view depends on demonstrating that the tethering wires have little aerodynamic effect; this has so far not been attempted, but a programme of tests is now being planned. Meanwhile, tethering wires have been used in the rig development tests described in this Report and will be used in a programme to measure hinge moment derivatives for an inboard control surface. In the latter tests, it will be reasonable to assume that wires at the wing tip will not have any significant effect on the control derivatives.

3.2 Excitation system

It is desirable to excite the control surface system with an oscillatory torque in order to avoid directional force inputs. Although a rotary exciter is ideally suited to the application, it is easier, in practice, to use two matched linear electromagnetic exciters operating at equal distances from the hinge line. The ready availability of such exciters simplifies the maintenance of the excitation system.

3.3 Response-measuring equipment

A single transducer, measuring displacement, velocity or acceleration at some point on the control surface system, is, in theory, the only instrumentation required on the rig. The signal from the transducer must be analysed and its variation with frequency presented in the form of a vector plot; this process is quite standard and merits no further discussion here. Needless to say, the overall calibration of transducer and analysis equipment must be made to a high order of accuracy, although it should be noted that an absolute

measurement of the amplitude of motion is not required in extracting resonance frequency and damping from a vector plot. It would be unwise, particularly in view of what was said about unwanted motions in section 3.1, to restrict the measurements to rotation of the control surface. Some check must be made on the motion at the outer end of the control and on the wing, either by accelerometers buried within the aerodynamic contour or by strain gauges at the wing root.

4 DETAILS OF RIG AND LABORATORY TESTS

4.1 Wing and control surface

In order to obtain a working rig as quickly as possible to demonstrate the validity of the technique, an existing wing model, designed for steady aerodynamics measurements, was modified so that a hinge control surface replaced the fixed control of the original. An outline of the rig arrangement is shown in Fig.2 and the wing geometry in Fig.3; the wing was built of solid steel but had spanwise and chordwise recesses which had been used to accommodate tubing in pressure plotting measurements. The control surface extended from root to tip (apart from a light alloy tip fairing which was carried on the wing) and its chord was 0.26 of the wing chord, with the hinge line at the leading edge of the control. The structure of the control consisted of leading edge and trailing edge spars joined by skins forming the upper and lower surfaces: the spars and skins were all moulded in carbon fibre reinforced plastic. Morganite Type I carbon fibre was used throughout, with a nominal 60% packing fraction and using a cold-setting resin. The centre of the control was filled with a rigid lightweight plastic foam to stabilise the skins. A plastic membrane of Melinex, 0.06 mm thick, sealed the gap between wing and control surface; the membrane was cast into the leading edge spar of the control and was held in the wing by a clamp. The two 20 swg steel tethering wires passed through holes at 17% and 43% chord in the wing tip fairing, and motion was prevented by locking screws. The arrangement is shown in Fig.4. The wing tip also carried a hardened steel pin seating in a wound carbon fibre reinforced plastic bearing let into the outer end of the control front spar. A splitter plate was fitted at the wing root as shown in Figs.5 and 6.

4.2 Rig

The front spar of the control surface extended inboard of the wing root, and was bonded into a light alloy cross-spring support system arranged so that the cross-spring axis coincided with the control surface hinge line.

Thus the control was supported by a cross-spring hinge just inboard of the wing root and by the tip fairing pin described in section 4.1. One end of the torsion bar providing the control stiffness was attached inboard of the cross-spring, the other end being firmly anchored to the tunnel structure. Two Ling Altec electromagnetic exciters (model V 202) were positioned so as to apply a torque to the outboard end of the torsion bar. A drawing of the rig is shown in Fig.7.

Rotation of the control was monitored by an accelerometer on the cross-spring support system and by strain gauges on the torsion bar.

4.3 Laboratory tests

The rig was resonance tested to establish the proximity of unwanted modal frequencies to the operating frequency and to measure the rotational inertia in the operating mode.

With the tethering wires attached to the wing tip no natural frequencies of the system were found below the operating frequency of 250 Hz. The lowest wing mode frequency was above 350 Hz.

The rig inertia was measured by adding small masses and measuring the change of frequency of the operating mode. From the rate of change of frequency with added mass, the rig moment of inertia was calculated to be $I = 0.000241$ kg m^2. This value of I includes the aerodynamic inertia appropriate to the laboratory atmospheric pressure. Using the results of the wind tunnel tests, at zero airspeed, described in section 5.1, a correction can be applied to the measured I to obtain the purely structural inertia which is required in equations (11) and (12). This correction is small and reduces the measured value of I by 0.4 per cent.

5 WIND TUNNEL TESTS

5.1 Range of test conditions

Calibration tests were made to establish the *in vacuo* natural frequency (ω_0) and damping (μ_0) for use in equations (11) and (12). These characteristics were measured over the range of tunnel pressures covered by the main tests, but with zero tunnel velocity. The resultant curves are shown in Fig.8, from which it may be seen that both natural frequency and damping vary with tunnel pressure. The curves of Fig.8 have been used to derive the *in vacuo* values of ω_0 and μ_0 (which are required in equations (11) and (12)) by extrapolating the curves to zero pressure.

It may be seen in Fig.8 that frequency measurements at different stages of the tests gave different results, the maximum differences being approximately 0.3 Hz. Because it would have been almost impossible to have evaluated a variation of ω_0 appropriate to every test condition, it was decided to use a fixed value of ω_0 which was obtained by extrapolating the mean values of resonance frequencies to zero pressure. The effect of errors in ω_0 and μ_0 is discussed in section 7.2.

Initial wind-on tests were made at M = 0.61 over a range of tunnel pressures, and were followed by similar series at M = 0.7, 0.8, 0.84, 0.88, 0.92, 0.96, 1.00, 1.05, 1.1 and 1.2. Because of tunnel limitations, a constant range of pressure could not be obtained at all Mach numbers; in practice, test conditions were chosen so that the effect of Reynolds number could be assessed over the Mach number range. Reynolds numbers of 0.7 to 2.7 million (based on wing mean chord) were covered in the range $0.6 < M < 0.95$, and 0.7 to 1.0 million in the range $0.95 < M < 1.2$.

5.2 Test procedure and data acquisition

The procedure in each test condition was to excite the control system with a constant sinusoidal force input at a number of discrete frequencies giving a control rotational amplitude of between 1 and 2 degrees. The frequency range covered the resonance of the system, and, in general, constant increments of frequency were chosen. At each frequency, the response of the control system was measured from the output of strain gauges on the torsion bar, the strain gauge signals being amplified and resolved into components in phase and quadrature with the force input. The resolved components were fed to an x-y plotter.

All the tests described in the Report were made in approximately twenty-six hours of tunnel running.

5.3 Test results

The test results consist of a vector response diagram for each tunnel condition. The diagrams are analysed to obtain the natural frequency (ω_r) and damping (μ_r) for use in evaluating equations (11) and (12). The calibration tests yield values for the wind-off conditions and were used to obtain ω_0 and μ_0 as described in section 5.1. An early indication of the quality of the test results may be gained by examining the shape of the vector response locus and the disposition of the plotted points in relation to one another and to the force input. Ideally for small damping the response locus will be very nearly circular and will be tangential to the force vector at the origin;

the maximum rate of change of the phase angle between force and response will occur at the natural frequency and this frequency will correspond to a phase angle of $\pi/2$. The extent to which a response diagram approaches the ideal can only be found after a detailed analysis is made, but experience makes it possible to judge from inspection whether the test results are of good or poor quality, and this is useful evidence to guide the detailed pattern of the test conditions.

The great majority of the vector response diagrams obtained from the tests were of excellent quality; typical diagrams may be seen in Figs.9 and 10. A few diagrams were somewhat less satisfactory, and these were invariably associated with conditions of nearly zero damping.

6 WIND TUNNEL DATA ANALYSIS

6.1 Vector plot analysis

The conventional method of analysing a circular vector plot is firstly to determine the resonance frequency from the point of maximum spacing between plotted points at equal frequency increments, and then to determine the damping from the change of frequency between two points equally spaced on each side of the resonance point. Referring to Fig.11, the resonance frequency ω_r occurs when $\frac{ds}{d\omega}$ is a maximum, and the damping is given by

$$\mu_r = \left(\frac{\omega_A - \omega_B}{2\omega_r}\right) \cot \frac{\theta}{2}$$

where μ_r is the fraction of critical damping. (The values of ω_r and μ_r obtained in this way are close approximations to the true values and involve various assumptions, including that of small damping. The reader should consult, for example, Bishop and Gladwell[2] for a complete analysis.)

In practice, this method of determining ω_r and μ_r tends to ignore data points other than those close to resonance; this would not be of serious consequence in, say, analysing ground resonance test response curves, nor even in analysing flutter test data since the errors involved are not large. In the tests described here, however, it must be remembered that h_β is proportional to $(\omega_r^2 - \omega_0^2)$ and h_β is proportional to $(\omega_r\mu_r - \omega_0\mu_0)$ (equations (11) and (12)) and both these terms will be small differences of relatively large quantities. Clearly, it is important to use a method of analysis of

the vector plots which will treat each plot consistently and which makes full use of all the data available. Accordingly an analysis was used which depends on the relationship:-

$$\tan \bar{\phi} = \frac{2\mu_r(\omega/\omega_r)}{1 - (\omega/\omega_r)^2}$$

where $\bar{\phi}$ is the phase angle between force and displacement response, and ω/ω_r is the ratio of the excitation frequency (ω) to the resonance frequency (ω_r). It was assumed that there might be a phase shift ϕ_0 in the phase datum on a vector plot so that the above equation was re-written

$$\tan (\phi - \phi_0) = \frac{2\mu_r(\omega/\omega_r)}{1 - (\omega/\omega_r)^2}$$

where values of (ϕ,ω) are known for all points on the plot, and it is required to find ω_r, μ_r and ϕ_0 by the method of least squares (see Fig.12). It is assumed that all the points lie on the circle which has been drawn as the best fit of the plotted points. The analysis is given in Appendix A, and a computer programme was written to evaluate ω_r, μ_r and ϕ_0. Two points of interest emerged from the results; first, the 'least squares' analysis produced more consistent results for the poorer quality vector plots than the conventional analysis and second the datum phase shift rarely exceeded ±2 degrees, the greatest shift being associated with the lowest damping conditions. The generally small datum phase shift indicates that a close approximation to the resonance condition occurs when there is a quadrature phase relationship between force and response - which is what would be expected for a single degree of freedom system. The value of this information in the present context is that it tends to confirm that the motion is, in fact, in only one degree of freedom and that wing and control surface do not distort.

6.2 Evaluation of derivatives

Values of $(-h_\beta)$ and $(-h_{\dot{\beta}})$ were obtained from equations (11) and (12), and are plotted against Mach number in Fig.13 for several values of Reynolds number. Although tunnel conditions giving nominally constant Reynolds number were chosen at each test Mach number, some variation of Reynolds number occurred because of temperature variations. The values of Reynolds number shown in Fig.13 are therefore approximate. The values of both Reynolds

number and frequency parameter (which is also shown in Fig.13) are based on wing mean chord.

It may be seen that some of the curves in Fig.13 do not cover the full range of Mach number, resulting from a relative scarcity of data for M > 0.92; this is particularly regrettable in the case of the damping derivative h'_β which changes sign in the transonic region. Tests at the highest two values of Reynolds number (2.7 and 2.0 million) could not be made above M = 0.92 because of tunnel running restrictions, and lack of testing time prevented detailed investigations being completed at the lower Reynolds numbers. Where $(-h'_\beta)$ fell rapidly with increasing Mach number some care had to be exercised in approaching the chosen test condition to avoid a situation in which negative aerodynamic damping exceeded positive structural damping leading to self-maintained oscillations generally known as 'buzz'. Thus, when $(-h'_\beta)$ became negative, extra time was necessarily spent in exploring the stability of the system to avoid hazarding the rig in uncontrolled oscillations. It was this aspect of the tests that occupied rather more of the available test time than had been anticipated. The opportunity was also taken to allow a self-maintained oscillation to occur at M = 0.96; the oscillatory condition was held for some two minutes and measurements showed little variation of amplitude during this time. During close stroboscopic examination of the motion the wing appeared quite stationary.

7 DISCUSSION

7.1 The test rig described in this Report has been shown to meet the design aims that were set out in section 1. The rig proved simple to construct, it used standard instrumentation and associated equipment and it presented no difficulties in operation. There are, however, several ways in which it could be improved, and there are one or two outstanding questions that need to be resolved. The most important of these relates to the tethering of the wing in order to prevent unacceptably large wing motions. Some thought is now being given to the design of an experiment in which the aerodynamic effects of tethering wires can be assessed. The possibility of designing wings more suited to the experiment than the modified steel wing used in the recent tests is also being explored.

7.2 The variation of the natural frequency of the rig over the period of the tests (shown in Fig.8) made it difficult to establish a value of ω_0 appropriate to all test conditions. Fig.8 indicates that the scatter in ω_0

about the mean is approximately ±0.15 Hz. To assess the effect of errors of this order, h_β and $h_\beta^\bullet$ were evaluated with ω_0 increased and decreased by 0.15 Hz. The opportunity was also taken to assess the effect of increasing and decreasing μ_0 by 10 per cent, and the results of both these investigations are shown in Fig.14, for the tests at Re = 0.7×10^6. It will be seen that the variation of ω_0 by ±0.15 Hz leads to a variation in $(-h_\beta)$ of approximately ∓ 0.007 at M = 0.6 falling to ∓ 0.005 at M = 1.2. The variation of ±10 per cent in μ_0 leads to a variation in $(-h_\beta^\bullet)$ of approximately ∓ 0.002 throughout the Mach number range. (The effect of ω_0 variation on $(-h_\beta^\bullet)$ is negligible, and $(-h_\beta)$ is independent of μ_0.) In future programmes, more care will be taken to establish accurate values of ω_0 and μ_0 by concentrating on calibration tests at low tunnel pressures and by more frequent checks on the variation of ω_0 and μ_0. It is not feasible, however, to make calibration checks more than two or three times in, say, a ten-hour period of tunnel testing, because of the time spent in changing the tunnel conditions.

7.3 On matters of testing technique there would seem to be some advantages in using a resonance-following system to maintain excitation at the natural frequency as the tunnel conditions are changed. Use of the RAE resonance test MAMA equipment[3] would enable the excitation frequency to be varied automatically so as to maintain a $\pi/2$ phase relationship between force and response. For each tunnel condition the vector plot would then be obtained by offsetting the demanded phase angle by equal increments above and below $\pi/2$. The procedure would give vector plots with many more points in the region of resonance than can easily be obtained when the tests are made in equal frequency increments, and the process should also be quicker.

7.4 Qualitatively, the values of $(-h_\beta)$ and $(-h_\beta^\bullet)$ obtained in the tests show the same general trends as those obtained in previous experiments[4], with a rise in the value of $(-h_\beta)$, and a rapid fall in the value of $(-h_\beta^\bullet)$ through the transonic region. The rate of change of both derivatives with Mach number is rather less than was expected from earlier work, and to some extent this simplified the experimental programme. The effect of Reynolds number on the stiffness derivative $(-h_\beta)$ is somewhat inconclusive, particularly transonically, though the value of the derivative tends to fall as Reynolds number is increased. The effect on the damping derivative $(-h_\beta^\bullet)$ is much more pronounced, the values becoming negative at lower Mach numbers as Reynolds number increases.

The values of Reynolds numbers in the tests were, of course, very low, and Fig.13 clearly demonstrates the need for tests at Reynolds numbers nearer full scale values.

The effect of Reynolds number on the $h_\beta^\bullet$ derivative is important, since previous tests have shown only a small effect. After studying all the available experimental data, Moore concluded[4] that, "with three-dimensional tests, the general effect on damping due to a change in Reynolds number ... appears to be small". Moore emphasised that his conclusions were tentative, and based on limited evidence; he stressed the importance of establishing the trends due to scale effects, and the results of the tests described here support his arguments for more experimental data to clarify the position.

7.5 Quantitatively, the derivative values are greater than was expected, although it is difficult to find experimentally-obtained values with which a valid comparison may be made. There are, in fact, few test results for combinations of $M \simeq 1$ and $\nu \simeq 1$. Such comparisons as can be made illustrate, only too clearly, that it is nearly impossible to take existing experimental data, and deduce derivative values for different planforms, Mach numbers and frequency parameters.

7.6 The minimum values of $(-h_\beta^\bullet)$ that can be measured depend on the test conditions. When the overall rig damping becomes zero, $\mu = 0$ in equation (11); hence

$$(-h_\beta^\bullet)_{min} = \frac{2I\omega_0\mu_0}{\rho V s c^3}$$

and this is the minimum value that can be measured (in the present experiments, $(-h_\beta^\bullet)_{min} \simeq -0.015$ in the transonic region). If it is necessary to explore the variation of $(-h_\beta^\bullet)$ further into the negative region, μ_0 must be increased. A general increase of μ_0 for the rig is unacceptable for the reasons given in section 2, but it may be feasible to add damping for particular test conditions, either by a damper on the rig or by injecting a damping torque through the exciters.

7.7 No attempt was made in the tests to maintain a constant maximum control amplitude for each resonance condition. This would be necessary if, for example, non-linearities were present. However, there was no indication from the response records of any non-linearity in the present series of tests and, for this reason, the effect of the amplitude of motion was not explored.

The absence of non-linearity is not a normal feature of control surface oscillatory behaviour and in general it would seem advisable to maintain constant control surface amplitudes in parametric investigations.

8 CONCLUSIONS

8.1 The use of a forced response and vector plot technique for the measurement of oscillatory aerodynamic control surface hinge moments enables these measurements to be made with a rig of simple design and standard instrumentation.

8.2 The main problem is that of preventing unwanted oscillatory motions of the aerofoil surfaces, in particular, bending distortion of the wing. Although this problem has been overcome by tethering the wing tip to the wind tunnel walls, it has yet to be shown that this solution is aerodynamically acceptable.

8.3 The results from a prototype rig show that consistent values of the direct hinge moment derivatives can be obtained quickly over a wide range of Mach number from subsonic to supersonic. Considerable care must be taken in establishing the still-air rig characteristics if significant errors in the derivatives are to be avoided.

8.4 Although the Reynolds numbers in the tests did not exceed 2.7 million, the effect of Reynolds number, particularly on the damping derivatives, was shown to be very significant, and it is evident that where derivative values applicable to full scale are required, tests must be made at more realistic values of Reynolds number.

8.5 Despite the need to check the validity of wing tethering as a means of preventing unwanted distortion, it is felt that the test technique described in this Report offers a relatively inexpensive and quick way of measuring direct control hinge moment oscillatory derivatives; these advantages make it attractive for project work where timescales are often too short for more conventional derivative measurement programmes.

Acknowledgements

The authors wish to thank Mr. K.H. Heron for making the analysis of Appendix A, and for programming it for computer solution. They also acknowledge the great help given by Miss P.K. New and Mrs. I.R. Levett during the tests, and the tunnel operating services provided by Aero Deparment, RAE.

Appendix A

ANALYSIS OF VECTOR RESPONSE CURVES

A.1 Referring to Fig.12 it is assumed that all the points lie on the circle which has been drawn as the best fit of the plotted points. The coordinates of each point P are expressed as (ω,ϕ), where ω is the excitation frequency, and ϕ is the phase angle between an arbitrary force datum through the origin, and the response vector measured from that datum. For a single degree of freedom system:-

$$\tan\ (\phi - \phi_0) \ = \ \frac{2\mu_r(\omega/\omega_r)}{1 - (\omega/\omega_r)^2} \qquad \text{(A-1)}$$

where ϕ_0 is the angle between the arbitrary and the true force datum,

μ_r is the fraction of critical damping for the system,

and ω_r is the undamped natural frequency

Values of ω_r, μ_r and ϕ_0 are required from a solution of equation (A-1) which gives the minimum error for all the measured points (ω,ϕ).

A.2 Re-writing equation (A-1) in the form:-

$$\left[1 - \left(\frac{\omega}{\omega_r}\right)^2\right] \sin\ (\phi - \phi_0) - 2\mu_r \left(\frac{\omega}{\omega_r}\right) \cos\ (\phi - \phi_0) \ = \ 0 \qquad \text{(A-2)}$$

and using the method of least squares, the error term e may be written:

$$e^2 \ = \ \Sigma\left[\left(1 - \left(\frac{\omega}{\omega_r}\right)^2\right) \sin\ (\phi - \phi_0) - 2\mu_r \left(\frac{\omega}{\omega_r}\right) \cos\ (\phi - \phi_0)\right]^2 \ = \ \Sigma[\Phi]^2 \qquad \text{(A-3)}$$

(say).

Hence

$$\frac{\partial e^2}{\partial \mu_r} \ = \ \Sigma[\Phi] \left(\frac{\omega}{\omega_r}\right) \cos\ (\phi - \phi_0) \ = \ 0 \qquad \text{(A-4)}$$

$$\frac{\partial e^2}{\partial \phi_0} \ = \ \Sigma[\Phi]\left[\left(1 - \left(\frac{\omega}{\omega_r}\right)^2\right) \cos\ (\phi - \phi_0) + 2\mu_r \left(\frac{\omega}{\omega_r}\right) \sin\ (\phi - \phi_0)\right] \ = \ 0$$

.... (A-5)

$$\frac{\partial e^2}{\partial \omega_r} = \Sigma[\Phi]\left[2\frac{\omega^2}{\omega_r^3}\sin(\phi-\phi_0) + 2\mu_r\frac{\omega}{\omega_r^2}\cos(\phi-\phi_0)\right] = 0 \qquad \text{(A-6)}$$

where the summations are made for all values of (ω,ϕ). (A-4), (A-5), (A-6) are three simultaneous equations from which ω_r, μ_r and ϕ_0 can be obtained. The procedure is to expand the equations so that they can eventually be written as follows. From equation (A-4):-

$$\omega_r^2(S_1\cos 2\phi_0 - C_1\sin 2\phi_0) - (S_3\cos 2\phi_0 - C_3\sin 2\phi_0) - 2\mu_r\omega_r(A_2 + C_2\cos 2\phi_0 + S_2\sin 2\phi_0) = 0 \ . \qquad \text{(A-7)}$$

From equation (A-5):-

$$\omega_r^4(S_0\cos 2\phi_0 - C_0\sin 2\phi_0) - 2\omega_r^2(S_2\cos 2\phi_0 - C_2\sin 2\phi_0) + (S_4\cos 2\phi_0 - C_4\sin 2\phi_0) - 4\mu_r\omega_r^3(C_1\cos 2\phi_0 + S_1\sin 2\phi_0) + 4\mu_r\omega_r(C_3\cos 2\phi_0 + S_3\sin 2\phi_0) - 4\mu_r^2\omega_r^2(S_2\cos 2\phi_0 - C_2\sin 2\phi_0) = 0 \ . \qquad \text{.... (A-8)}$$

From equation (A-6):-

$$\omega_r^2(A_2 - C_2\cos 2\phi_0 - S_2\sin 2\phi_0) - (A_4 - C_4\cos 2\phi_0 - S_4\sin 2\phi_0) - 2\mu_r\omega_r(S_3\cos 2\phi_0 - C_3\sin 2\phi_0) + \mu_r\omega_r^3(S_1\cos 2\phi_0 - C_1\sin 2\phi_0) - \mu_r\omega_r(S_3\cos 2\phi_0 - C_3\sin 2\phi_0) - 2\mu_r^2\omega_r^2(A_2 + C_2\cos 2\phi_0 + S_2\sin 2\phi_0) = 0 \qquad \text{(A-9)}$$

where $A_m = \Sigma\omega^m$

$S_m = \Sigma\omega^m \sin 2\phi$

$C_m = \Sigma\omega^m \cos 2\phi$.

Equation (A-7) gives $\mu_r\omega_r$ in terms of ω_r^2, and when this is substituted into (A-9), ω_r^2 can be expressed as a function of ϕ_0. (The sum of the last three terms of equation (A-9) is zero, from equation (A-7).) Thus

$$\omega_r^2 = \frac{P}{Q} \tag{A-10}$$

where $P = (A_2 + S_2 \sin 2\phi_0 + C_2 \cos 2\phi_0)(A_4 - S_4 \sin 2\phi_0 - C_4 \cos 2\phi_0)$

$- (S_3 \cos 2\phi_0 - C_3 \sin 2\phi_0)^2$

and $Q = (A_2 + S_2 \sin 2\phi_0 + C_2 \cos 2\phi_0)(A_2 - S_2 \sin 2\phi_0 - C_2 \cos 2\phi_0)$

$- (S_1 \cos 2\phi_0 - C_1 \sin 2\phi_0)(S_3 \cos 2\phi_0 - C_3 \sin 2\phi_0)$.

Again, substituting for $\mu_r \omega_r$ in terms of ω_r^2, from (A-7) into (A-8), and then substituting for ω_r^2 from (A-10), gives

$$RP^2 + SPQ + TQ^2 = 0 \tag{A-11}$$

where:-

$R = (S_0 \cos 2\phi_0 - C_0 \sin 2\phi_0)(A_2 + S_2 \sin 2\phi_0 + C_2 \cos 2\phi_0)^2$

$-2(S_1 \cos 2\phi_0 - C_1 \sin 2\phi_0)(S_1 \sin 2\phi_0 + C_1 \cos 2\phi_0)(A_2 + S_2 \sin 2\phi_0 + C_2 \cos 2\phi_0)$

$-(S_2 \cos 2\phi_0 - C_2 \sin 2\phi_0)(S_1 \cos 2\phi_0 - C_1 \sin 2\phi_0)^2$

$S = 2\{(S_1 \cos 2\phi_0 - C_1 \sin 2\phi_0)(S_3 \cos 2\phi_0 - C_3 \sin 2\phi_0)(S_2 \cos 2\phi_0 - C_2 \sin 2\phi_0)$

$+(S_1 \cos 2\phi_0 - C_1 \sin 2\phi_0)(S_3 \sin 2\phi_0 + C_3 \cos 2\phi_0)(A_2 + S_2 \sin 2\phi_0 + C_2 \cos 2\phi_0)$

$+(S_3 \cos 2\phi_0 - C_3 \sin 2\phi_0)(S_1 \sin 2\phi_0 + C_1 \cos 2\phi_0)(A_2 + S_2 \sin 2\phi_0 + C_2 \cos 2\phi_0)$

$-(S_2 \cos 2\phi_0 - C_2 \sin 2\phi_0)(A_2 + S_2 \sin 2\phi_0 + C_2 \cos 2\phi_0)^2\}$

$T = (S_4 \cos 2\phi_0 - C_4 \sin 2\phi_0)(A_2 + S_2 \sin 2\phi_0 + C_2 \cos 2\phi_0)^2$

$-2(S_3 \cos 2\phi_0 - C_3 \sin 2\phi_0)(S_3 \sin 2\phi_0 + C_3 \cos 2\phi_0)(A_2 + S_2 \sin 2\phi_0 + C_2 \cos 2\phi_0)$

$-(S_2 \cos 2\phi_0 - C_2 \sin 2\phi_0)(S_3 \cos 2\phi_0 - C_3 \sin 2\phi_0)^2$

and P and Q are defined above.

Equation (A-11) was solved iteratively on the computer to obtain ϕ_0; ω_r was then obtained from (A-10), and μ_r from (A-7), i.e.

$$\mu_r = \frac{(S_1 \cos 2\phi_0 - C_1 \sin 2\phi_0)\omega_r^3 - (S_3 \cos 2\phi_0 - C_3 \sin 2\phi_0)}{2(A_2 + S_2 \sin 2\phi_0 + C_2 \cos 2\phi_0)\omega_r} . \quad \text{(A-12)}$$

REFERENCES

No.	Author(s)	Title, etc.
1	-	Report of the working party on unsteady aerodynamics. ARC 31 398 (1969)
2	R. E. D. Bishop G. M. L. Baldwell	An investigation into the theory of resonance testing. Phil. Trans. Roy Soc. A 255 (No.1055), 241 (1963)
3	G. A. Taylor D. R. Gaukroger C. W. Skingle	MAMA - A semi-automatic technique for exciting the principal modes of vibration of complex structures. R & M 3590 (1967)
4	A. W. Moore	Scale effects on oscillatory control-surface derivatives. ARC CP 1151 (1969)

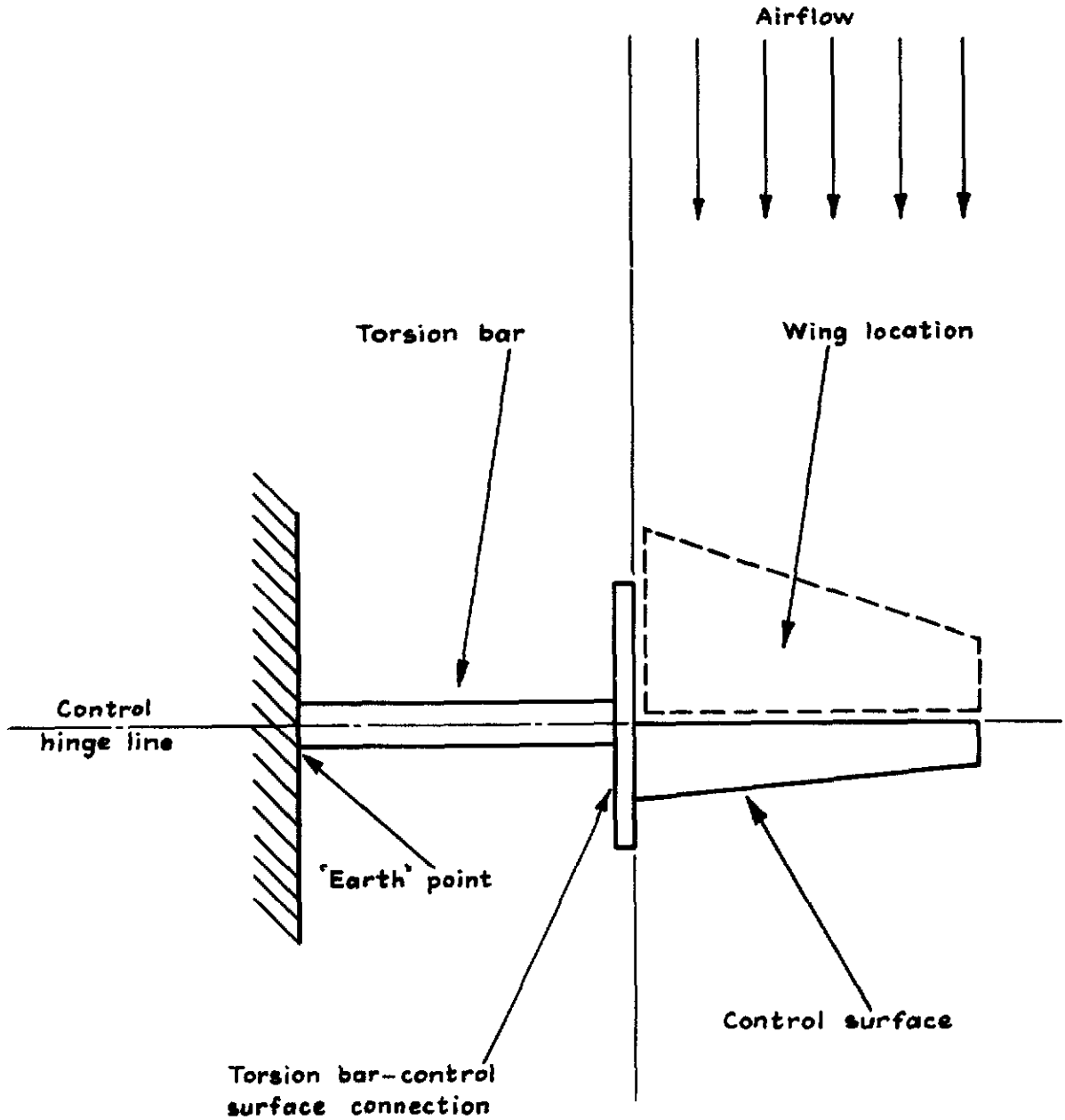

Fig. 1 Dynamic representation of rig

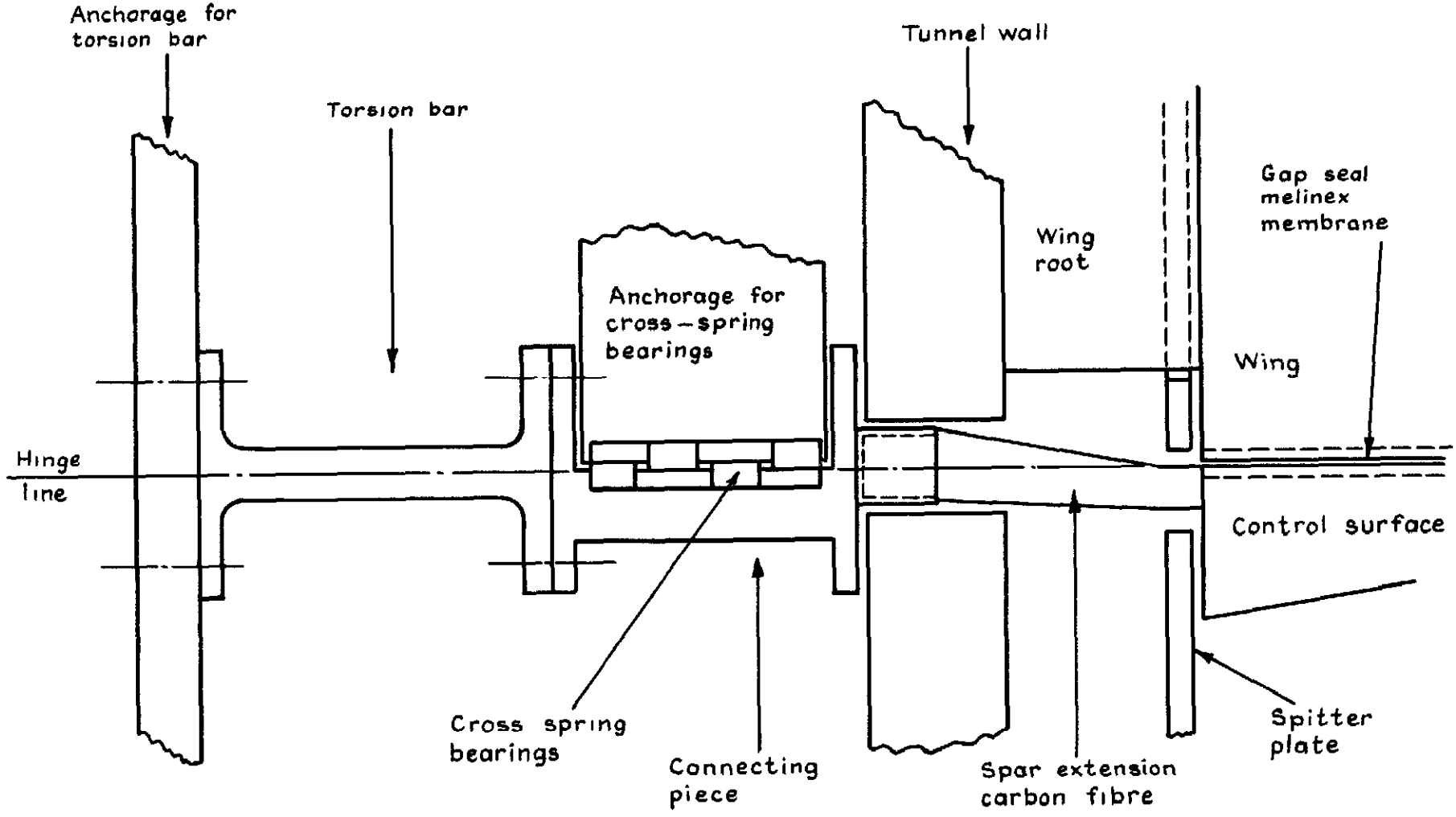

Fig. 2 Outline of rig arrangement

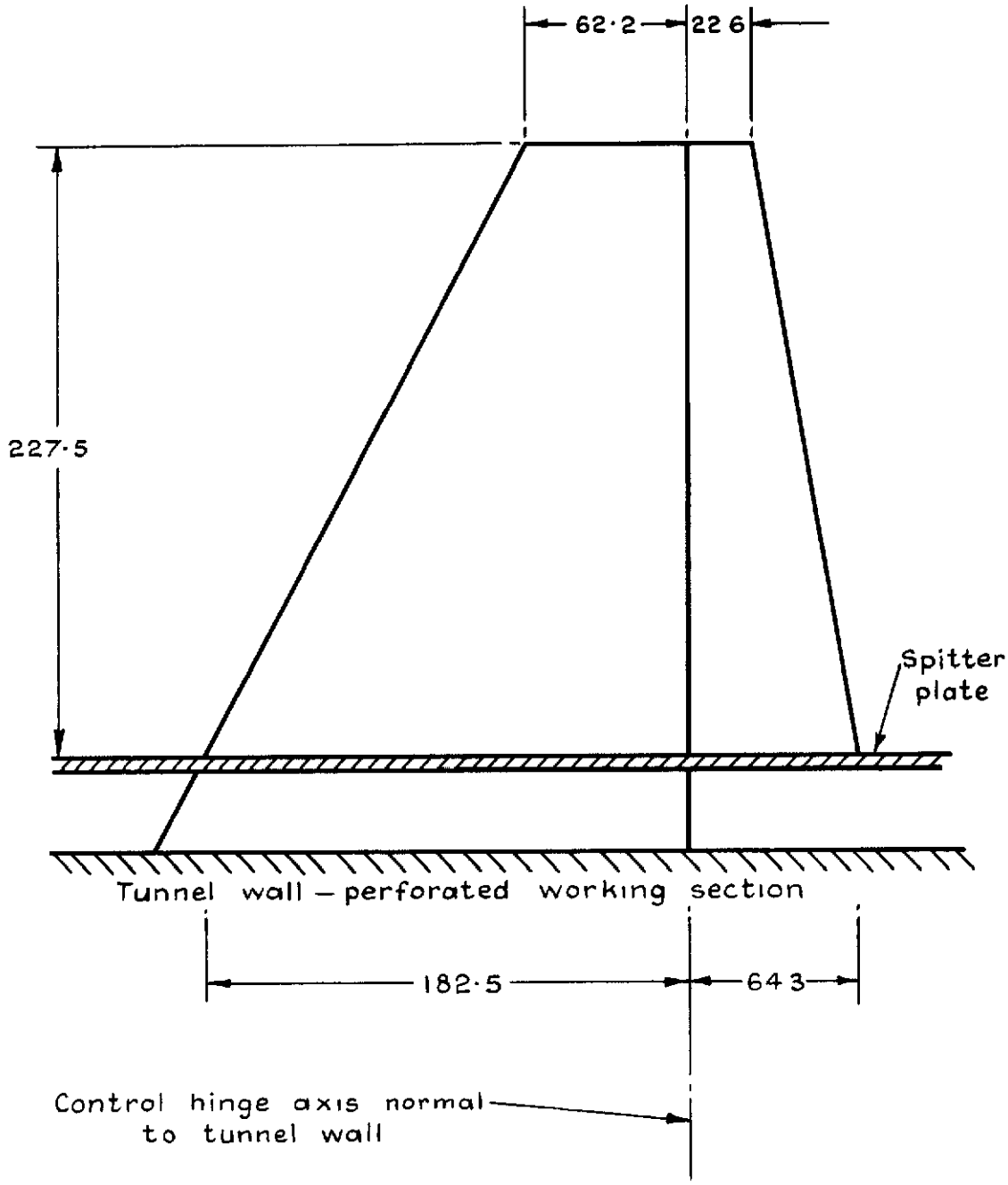

Aerofoil section RAE 102
$t/c = 0{\cdot}06$ $A = 2{\cdot}744$

Note.- Dimensions in mm

Fig. 3 Geometry of wing and control surface

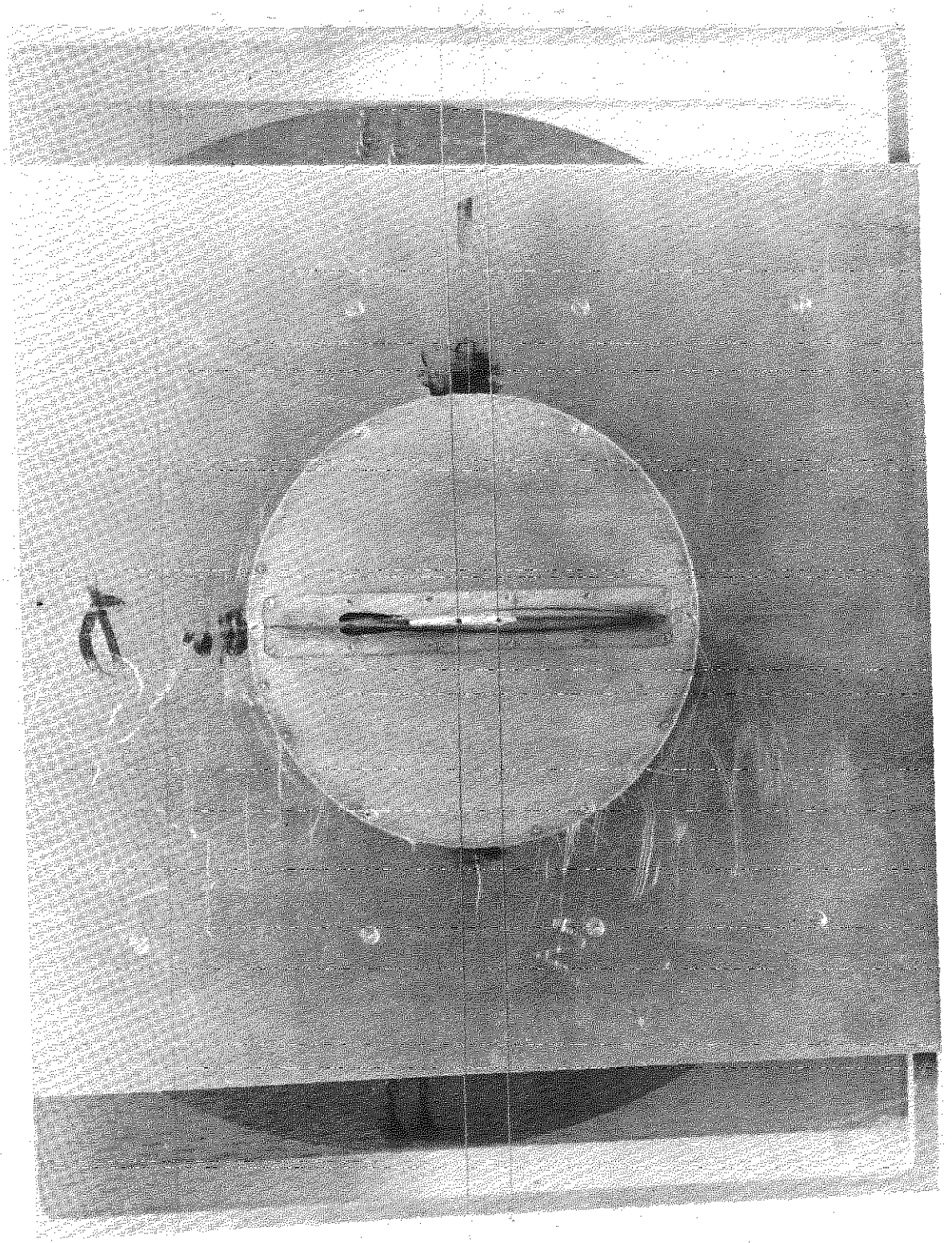

Fig.4. Arrangement of tethering wires

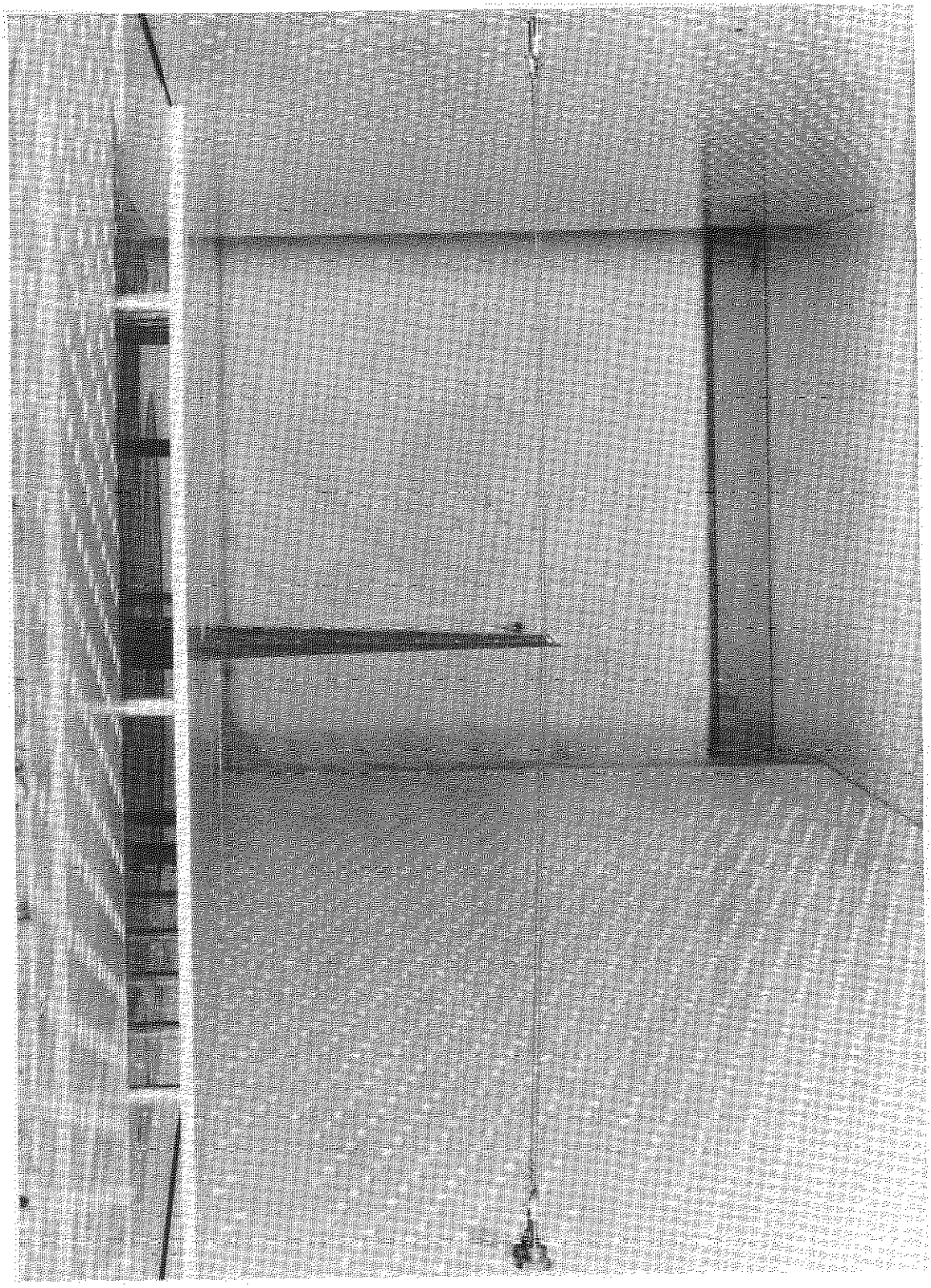

Fig.5. Arrangement of splitter plate

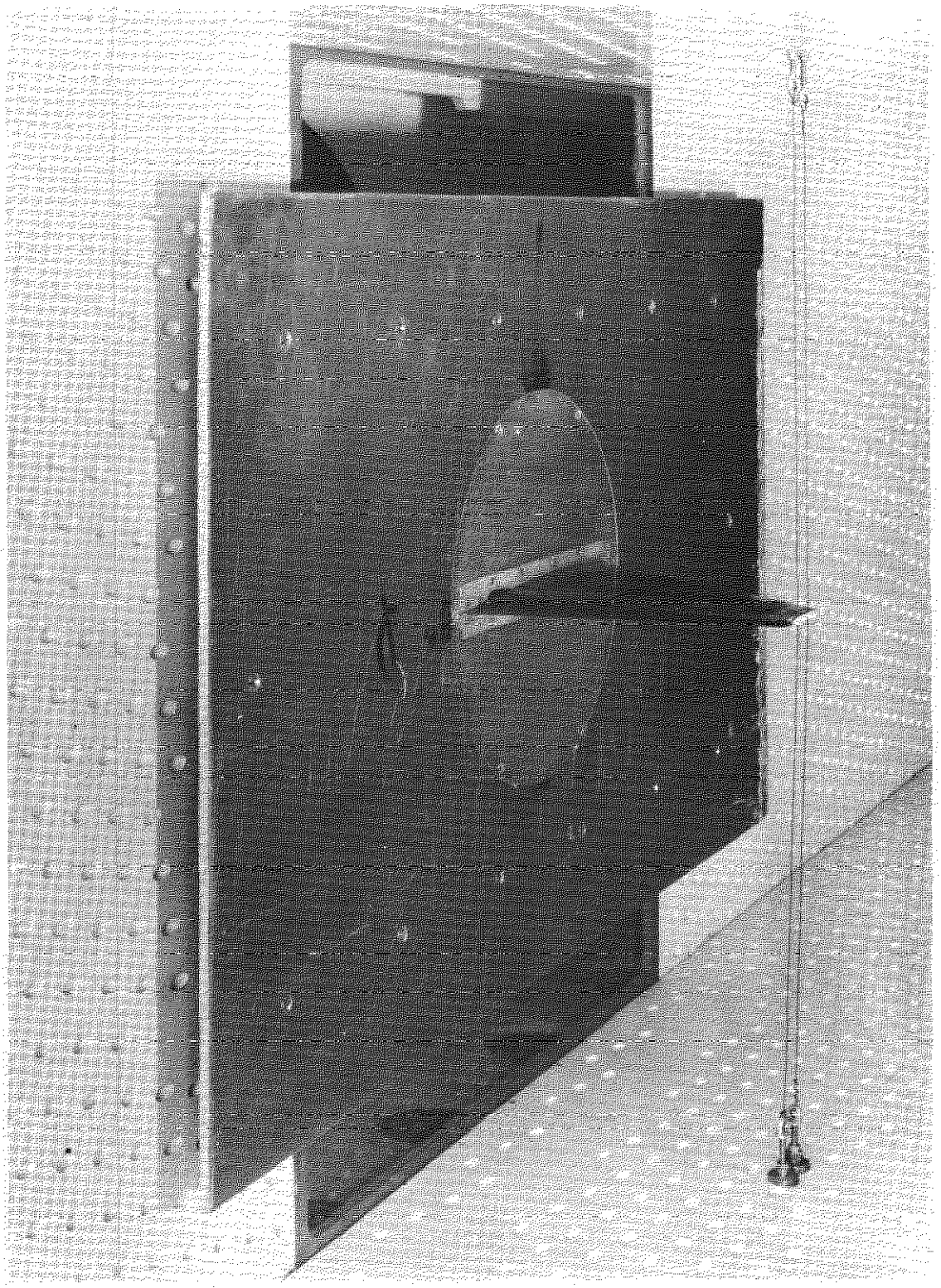

Fig.6. View of splitter plate and tethering wires

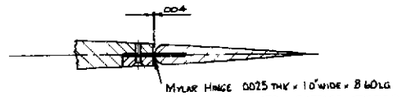

SECTION AA (NOT TO SCALE)

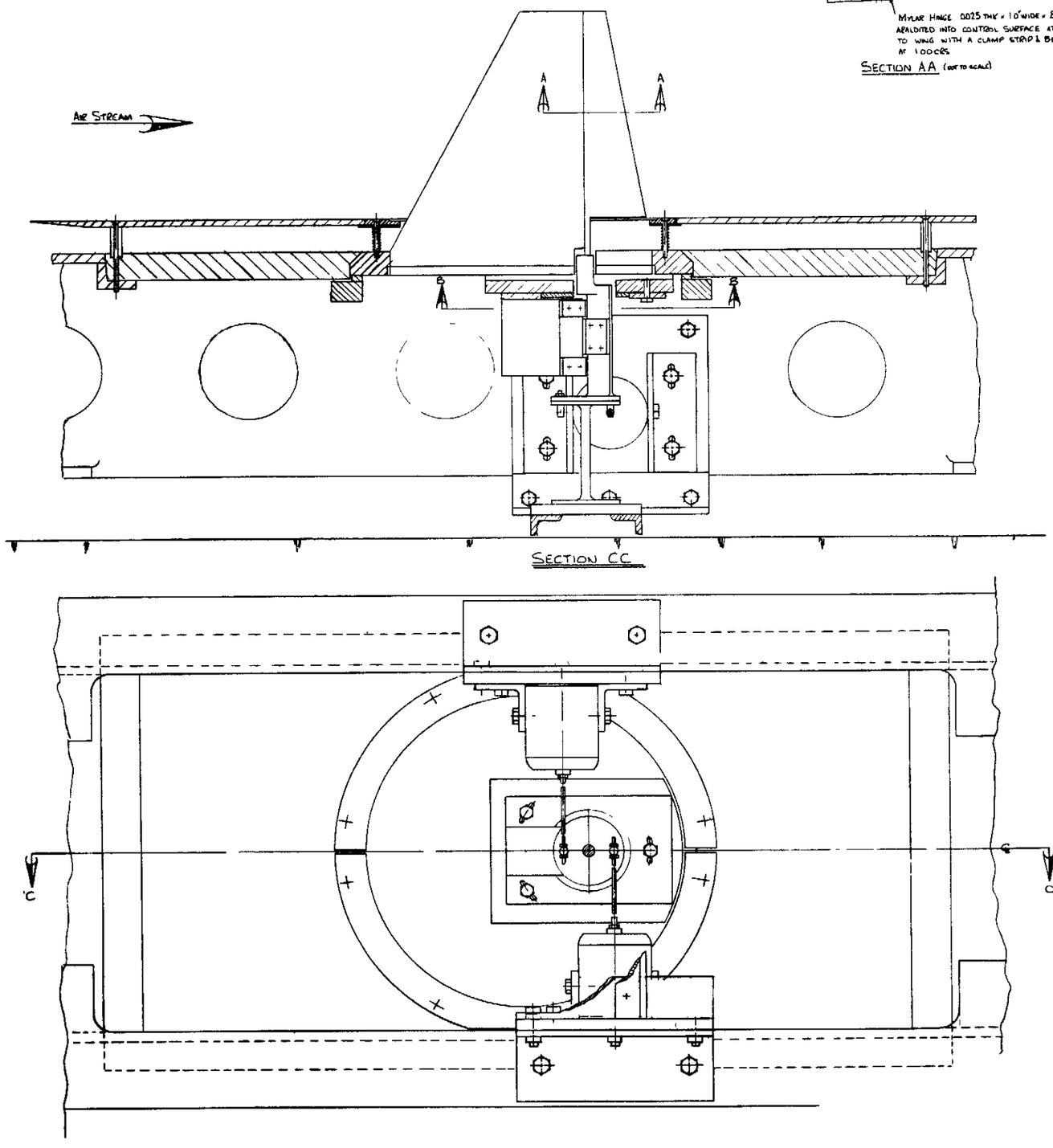

SECTION CC

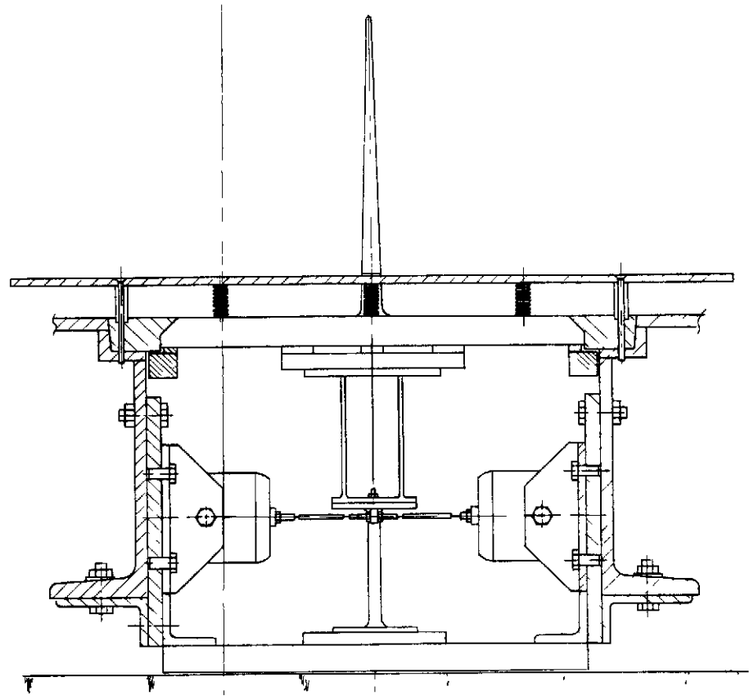

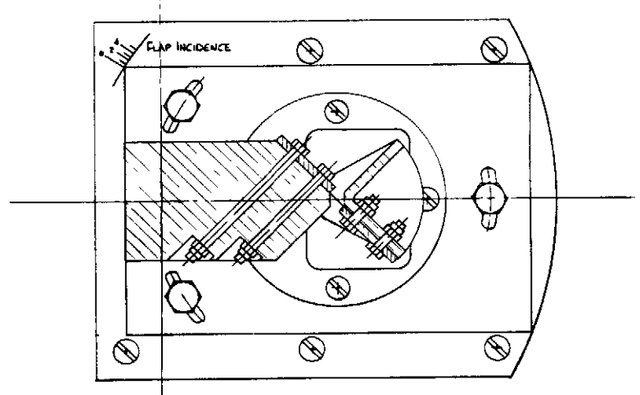

SECTION BB Scale ½

Fig.7. Detailed arrangement of rig

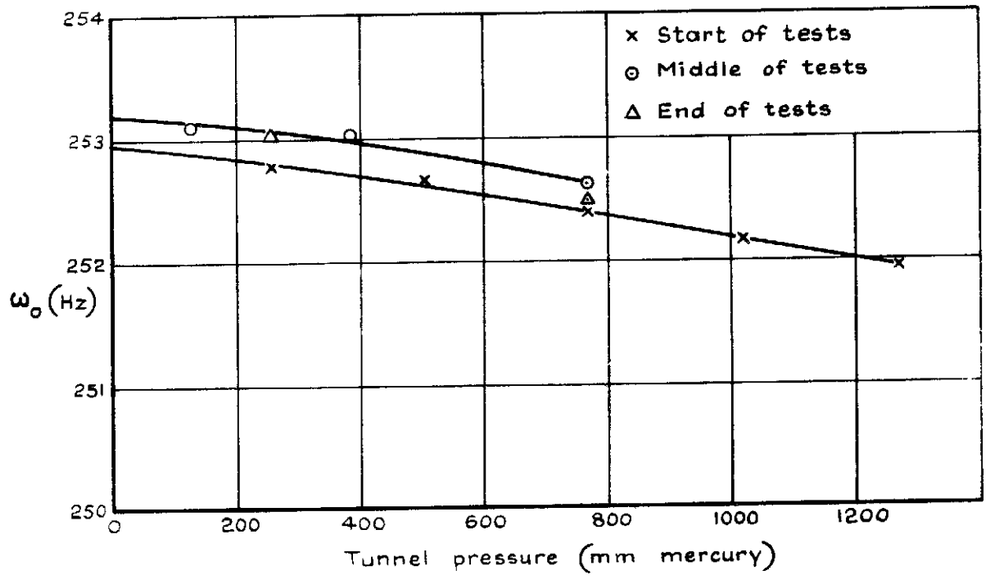

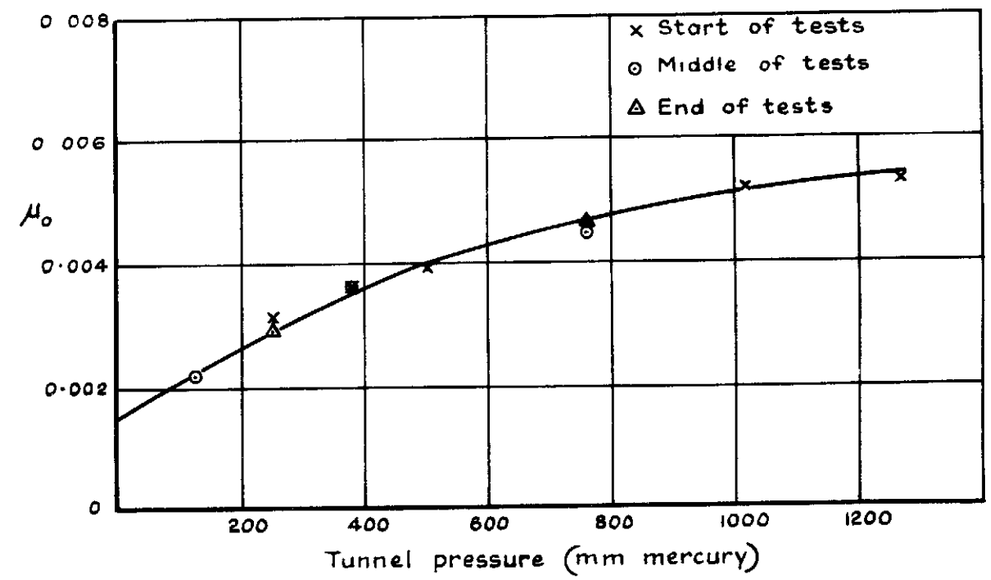

Fig. 8 Calibration tests at V=O

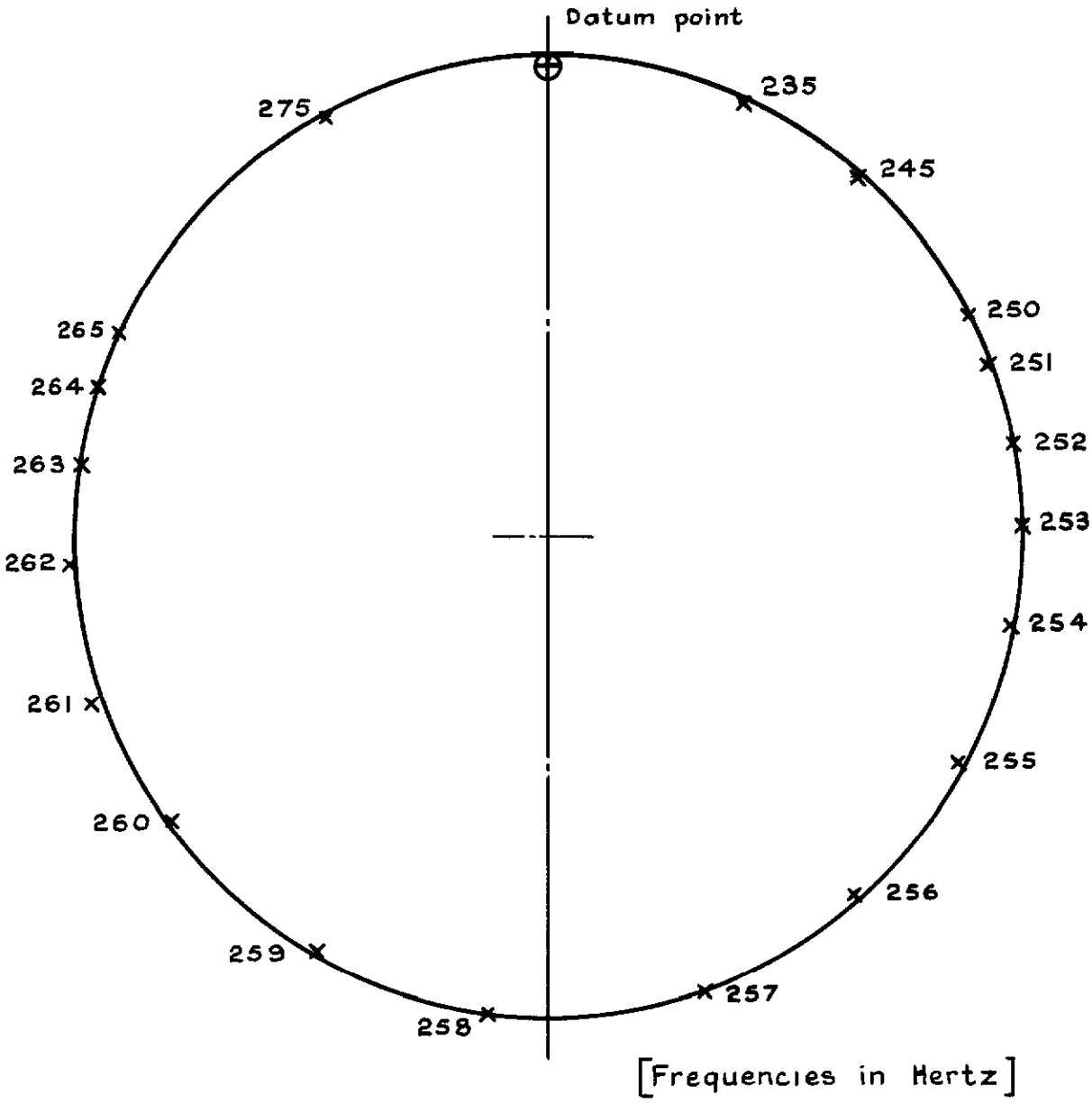

Mach No : 0·8

Reynolds No: $2 \cdot 0 \times 10^6$

Resonance frequency : 257·87 Hz

Damping : 0·0178 of critical

Fig. 9 Typical vector response curve

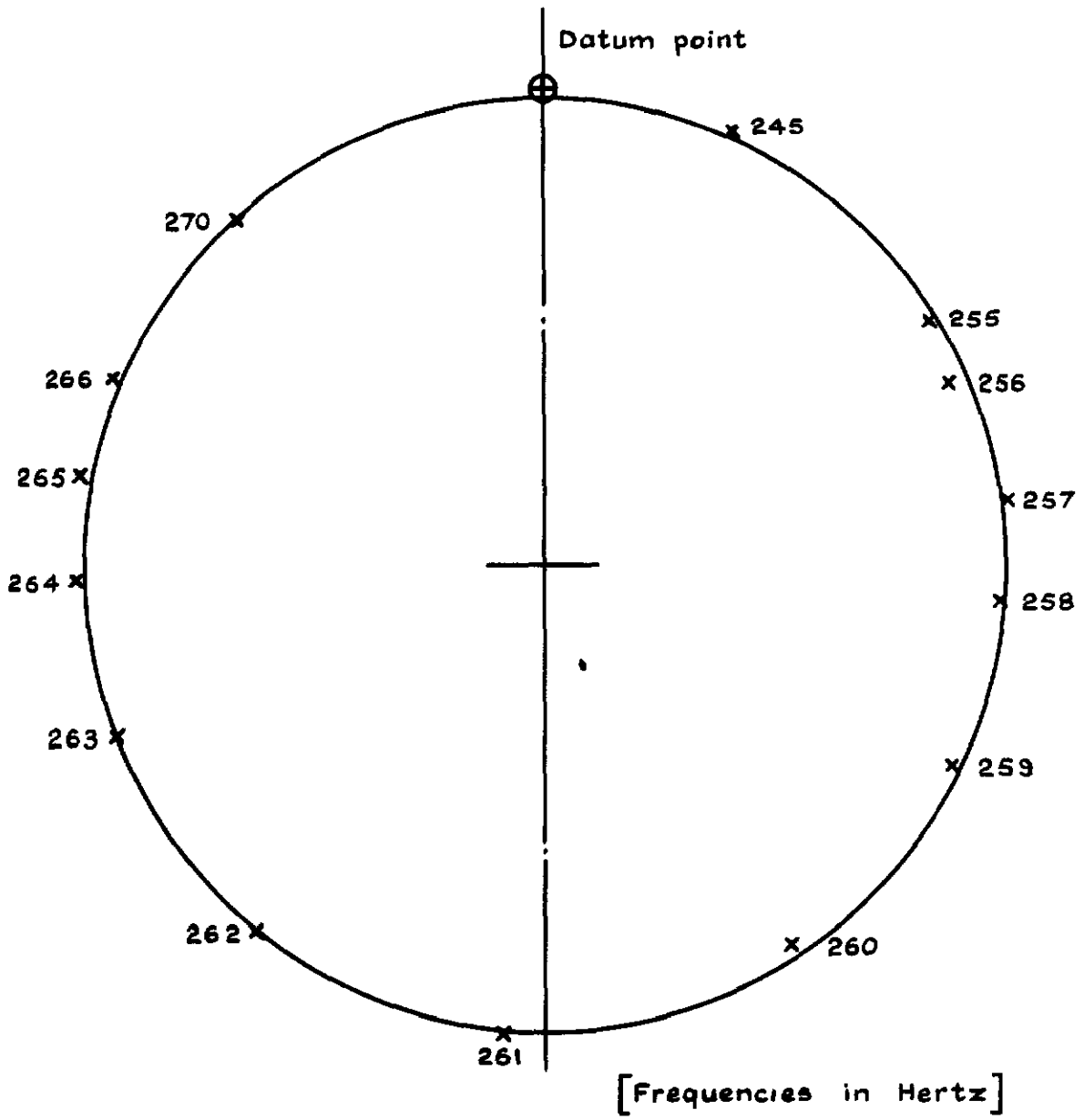

Mach No : 0·88

Reynolds No : $2 \cdot 7 \times 10^6$

Resonance frequency : 260·9

Damping : 0·0128 of critical

Fig. 10 Typical vector response curve

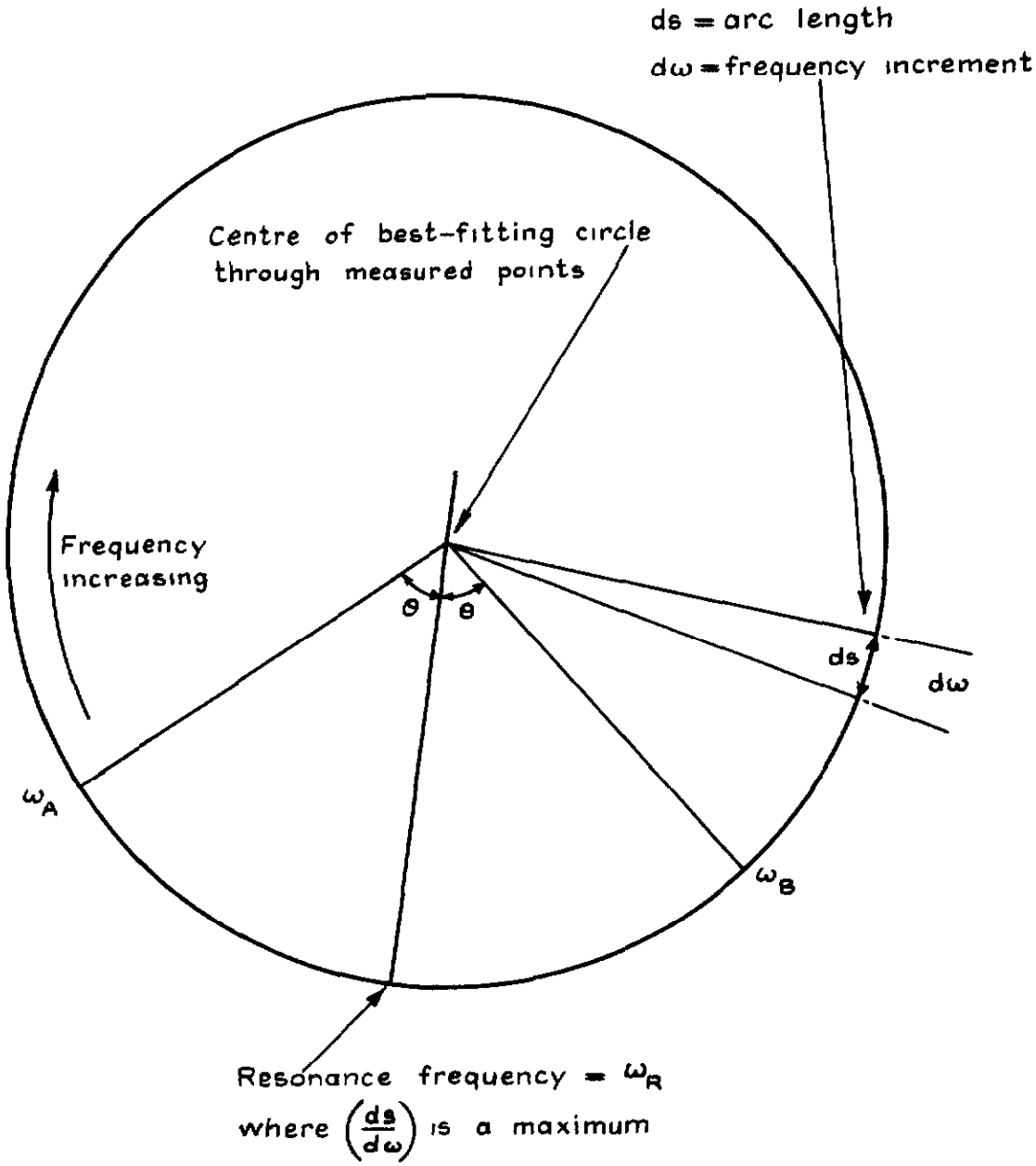

$$\text{Damping } \mu_r = \left(\frac{\omega_A - \omega_B}{2\,\omega_R}\right) \cot \frac{\theta}{2}$$

Fig.11 Graphical analysis of vector response curves

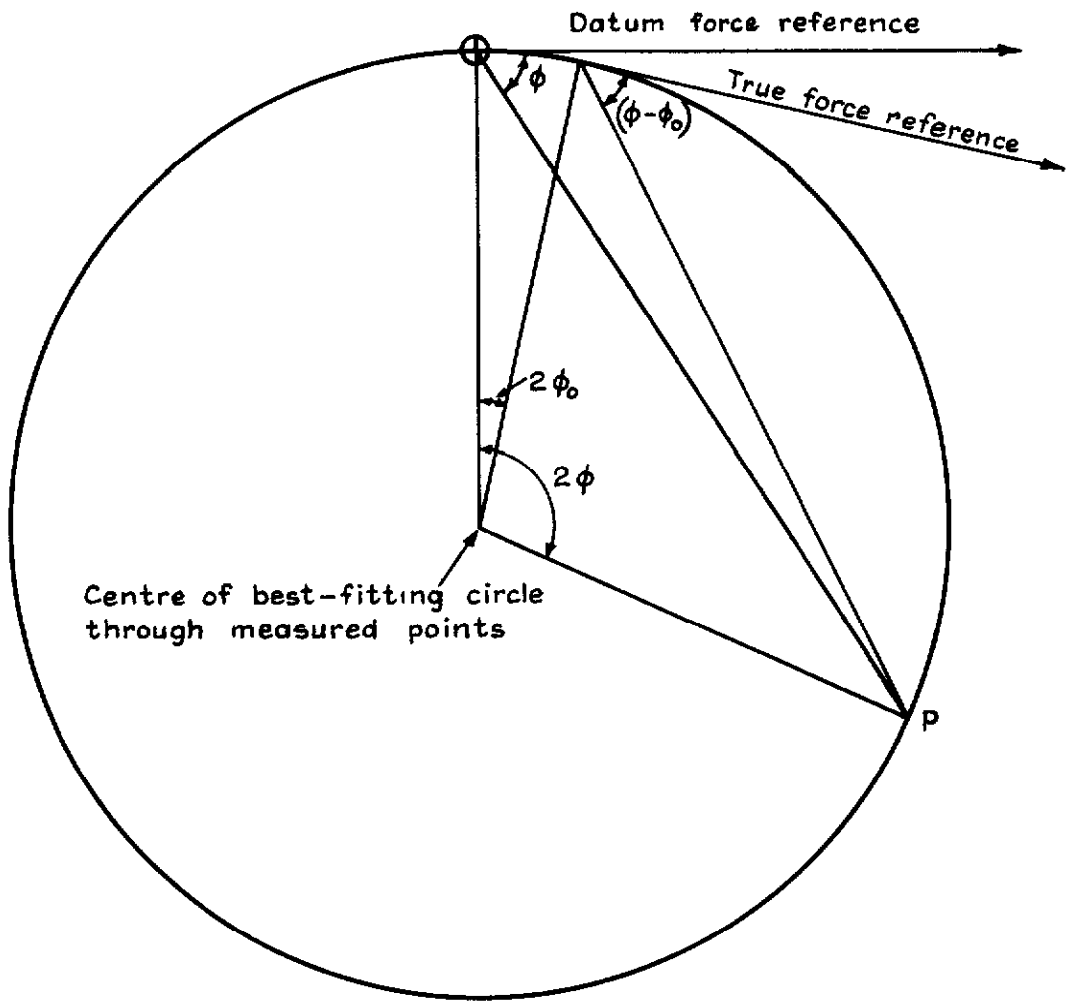

Coordinates of measured points P are (ω, ϕ)
Values of resonance frequency ω_R, damping μ_R and datum phase error ϕ_o are found by solving

$$\tan(\phi-\phi_o) = \frac{2\mu_R\left(\frac{\omega}{\omega_R}\right)}{1-\left(\frac{\omega}{\omega_R}\right)^2}$$

for all data points P, using the least squares method

Fig. 12 Computer analysis of vector response curves

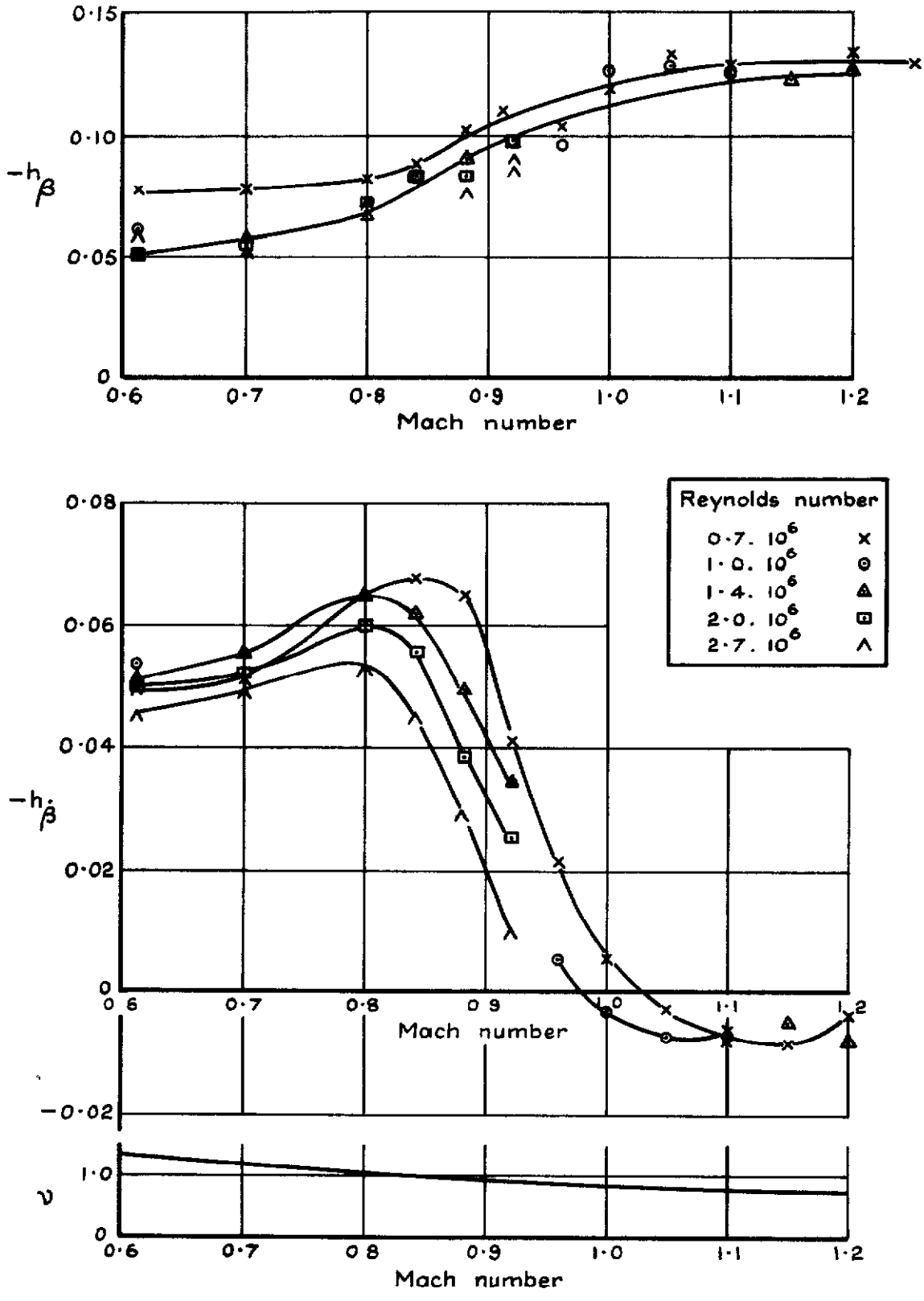

Fig. 13 Stiffness and damping derivatives

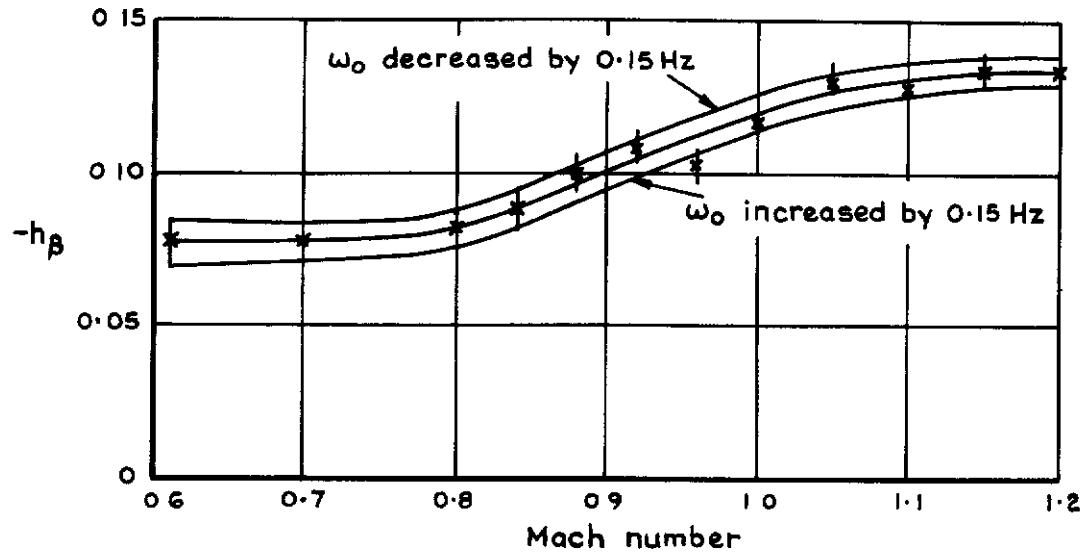

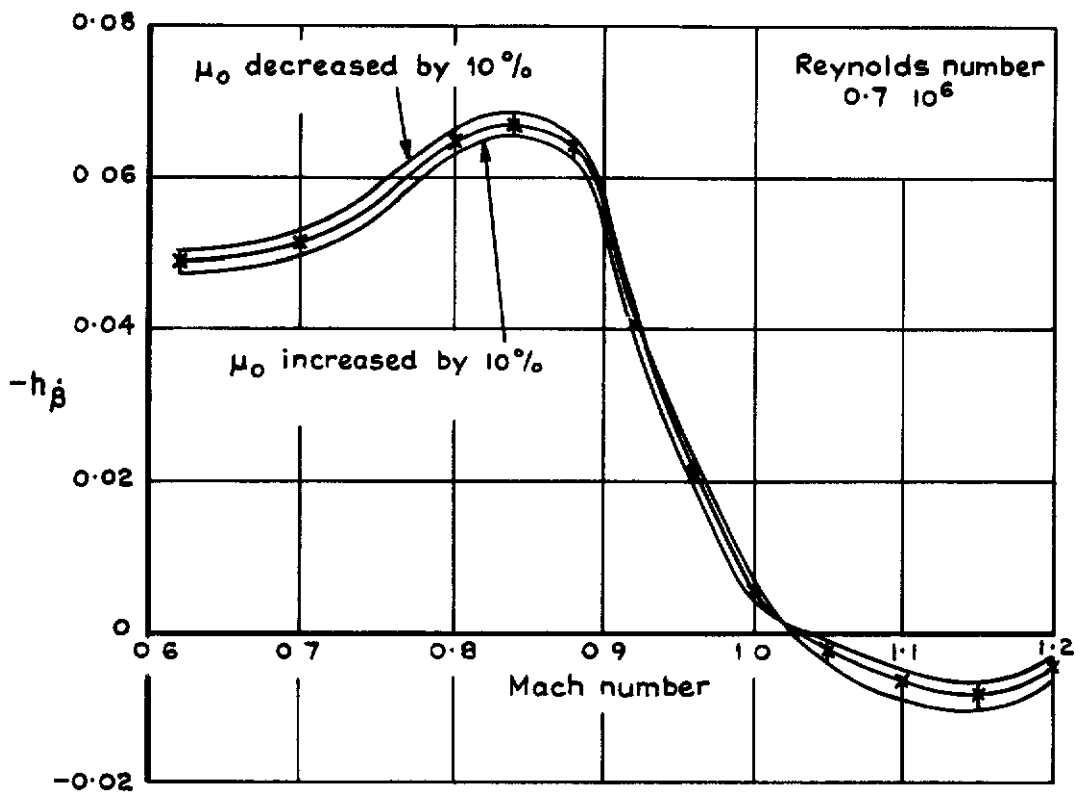

Fig. 14 Effect of errors in ω_o and μ_o on stiffness and damping derivatives

Printed in England for Her Majesty's Stationery Office by the Royal Aircraft Establishment, Farnborough Dd 505716 K4 6/73

Published by
HER MAJESTY'S STATIONERY OFFICE

To be purchased from
49 High Holborn, London WC1 V 6HB
13a Castle Street, Edinburgh EH2 3AR
109 St Mary Street, Cardiff CF1 1JW
Brazennose Street, Manchester M60 8AS
50 Fairfax Street, Bristol BS1 3DE
258 Broad Street, Birmingham B1 2HE
80 Chichester Street, Belfast BT1 4JY
or through booksellers

C.P. No. 1253

SBN 11 470811 8